Mechanism of Degradation of an α- Keto-Epoxide, PIV-PR-020: A Model for the Warhead for Various Proteasome Inhibitor Anticancer Agents

By

Kaci Phizackerley

Submitted to the graduate degree program in
Pharmaceutical Chemistry and the Graduate Faculty of
the University of Kansas in partial fulfillment of the
requirements for the degree of Master's of Science.

Chairperson _____
Valentino J. Stella

Committee Members _____
John Stobaugh

_____
Mouhannad Jumaa

Date
Defended_____

The Thesis Committee for Kaci Phizackerley certifies
that this is the approved Version of the following thesis:

Mechanism of Degradation of an α- Keto-Epoxide , PIV-PR-020: A Model for the Warhead for Various Proteasome Inhibitor Anticancer Agents

Chairperson _____
Valentino J. Stella

_____
Date Approved

ABSTRACT

Proteasome inhibitors are clinically effective treatment of multiple myeloma and mantle cell lymphoma. One proteasome inhibitor already on the market and one under clinical investigation are epoxy-ketones that potently and irreversibly bind to the proteasome. Kinetics were studied by loss of an α-keto-epoxide, PR-020 Pivoyl (PIV-PR-020), a model for the warhead of a number of proteasome inhibitor anticancer agents, namely, carfilzomib and oprozomib, in aqueous solutions as a function of pH, temperature and solvent composition.

The loss of PIV-PR-020 followed pseudo first order kinetics and provided a U-shaped pH-rate profile with an apparent pH-independent region between pH values of approximately 4 to 7. The degradation of PIV-PR-020 in aqueous solution was found to be both acid catalyzed below pH 4 and base catalyzed above pH 7. During the course of the study, the temperature, ionic strength, buffer concentration, and halide effect were evaluated while keeping the concentration of the reactant constant. Under acidic conditions, as you increase the halide nucleophilicity, the reactivity increases. The α-keto-epoxide ring opening in an SN_2 reaction under acidic conditions and is undefined under basic conditions. It has also been shown that there is some scrambling at the carbon at the C_1 position at higher pH values due to base catalyzed isomerization, and there is evidence that this diastereomer further degrades to a diol. At pH 8, the rate equations are complex due to reversible and parallel reactions. The study of PIV-PR-020 provides insight into the likely routes and rates of degradation at the warhead of carfilzomib and oprozomib.

Acknowledgements

I would like to acknowledge the teaching, support, and counsel of Professor Valentino Stella and the education and assistance I received from the rest of University of Kansas Pharmaceutical Chemistry Department faculty and staff. I would also like thank Dr. Mouhannad Jumaa for all of the support, guidance, and advice provided throughout this study. I would also like to thank Onyx Pharmaceuticals, and all of my colleagues, especially Dr. Mary Price for her guidance in the HPLC method development, and Dr. Bradley Wolfe for the generation of the PIV-PR-020 compound, and the degradation products, and Huy-Thahn Le for the endless supply of mobile phase and HPLC technical support, and Dr. Christopher Ablan for interesting talks on degradation pathways and LCMS assistance. Lastly, I would like to thank my friends and family for their support throughout this whole program, specifically my husband Keith and my children Drew and Addison, who always are there to help out and support me throughout this journey.

Table of Contents

PURPOSE

The purpose of this research is to investigate the reactivity, kinetics and mechanism of loss of an α-keto-epoxide, PR-020 Pivoyl (PIV-PR-020), a model for the warhead of a number of proteasome inhibitor anticancer agents, in aqueous solutions as a function of pH and solvent compositions at varying temperatures.

INTRODUCTION

PIV-PR-020 with the (S,R) S(C_1), R (C_3) stereochemistry (Figure 1) contains the α keto-epoxide functional group, the warhead group for both carfilzomib, also known as Kyprolis®, and the oral follow on drug, oprozomib (1).

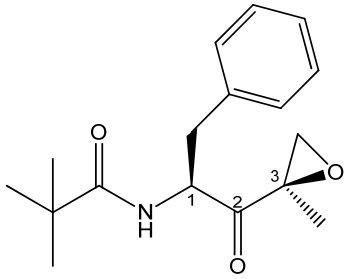

Figure 1. PIV-PR-020 with the (S,R), (S (C_1), R (C_3)) stereochemistry

Proteasome Inhibitors, carfilzomib and oprozomib, are peptide epoxiketones (Figure 2), which are potent and irreversible anticancer agents used to treat multiple myeloma. Proteasome inhibition has been proven to be clinically effective in the treatment of multiple myeloma and mantle cell lymphoma. Two proteasome inhibitors already on the market are carfilzomib (Kyprolis®) and bortezomib, a dipeptide boronic acid (2; 3). A naturally occurring tetra-peptide epoxy-ketone, epoxomicin, selectively, potently and irreversibly inhibits proteasome activity in the 20S proteasome (4; 3). Both bortezomib and carfilzomib are already approved for the treatment of multiple myeloma with

biweekly IV dosing. Oprozomib, a carfilzomib analog, is under clinical evaluation in phase II as an oral proteasome inhibitor. An oral drug would provide flexibility and convenience in dosing and ultimately improved patient quality of life (2).

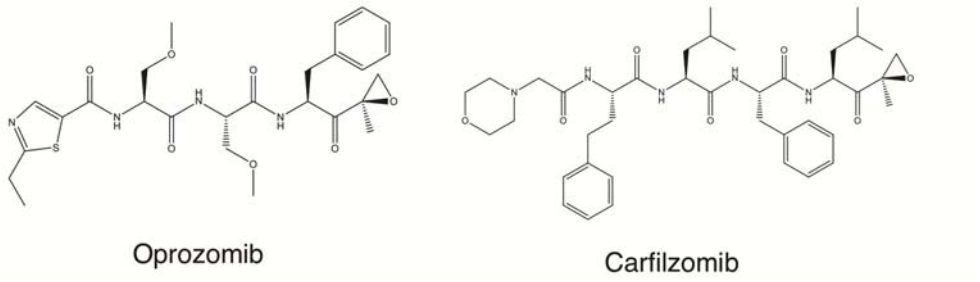

Figure 2. Structure of oprozomib and carfilzomib

Carfilzomib and oprozomib are small molecules with modest molecular weights and both have multiple chiral carbons, as shown in Figure 2 (3). PIV-PR-020 is an α-keto-epoxide with only one amino-acid mimetic group, and has two chiral carbons at the C_1 and C_3 positions (see Figure 1). PIV-PR-020 also has relatively high solubility in aqueous media over the pH range of interest and a chromophore UV detectable by HPLC at concentrations at one tenth of its solubility, enabling this stability study. Since the chemical reactivity of α-keto-epoxides is of interest in this study, to minimize complications from degradation other than at the warhead, PIV-PR-020 was chosen for a more in-depth chemical stability study. Therefore, this study will investigate the degradation kinetics of PIV-PR-020 as a function of pH, temperature, buffer strength and the effect of halides and its degradation product profile.

Epoxides

Although there has been an increase in literature references on the chemical reactivity of simple epoxides (5), the majority of the literature over the past 80 years is primarily focused on epoxide-containing resins. More recently, simple epoxides have proven to be useful to synthetic chemists as intermediates employed in drug development (6). The attraction of epoxides for synthetic chemists are mainly for obtaining high degree of stereo-chemical and regio-chemical purity when reacted with a nucleophile. However, these reactions often employ commercially unavailable reagents, expensive catalysts and/or severe conditions (7; 8; 6).

Reactivity of Keto-epoxides

Epoxides are more reactive than simple ethers due to inherent ring strain and react with nucleophiles resulting in ring opening. (Figure 3). (9; 10)

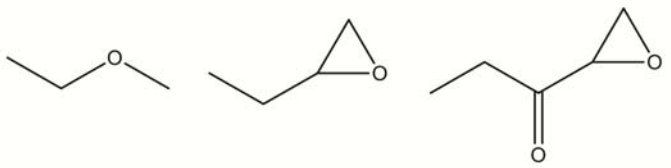

Figure 3. Structures illustrating a simple ether (left) and epoxide (middle) and an α-keto-epoxide

Hydrolysis of epoxides is well known and occurs readily at acidic pH values. (11; 10) At a low pH environment, the epoxide oxygen is partially protonated and can be readily attacked by a nucleophile at the less sterically hindered site, resulting in

epoxide ring-opening (Scheme 1). This reaction in the low pH environment is an SN_2 reaction, concerted reaction, but can also occur via a SN_1 reaction depending on the structure of the epoxide. (11; 10)

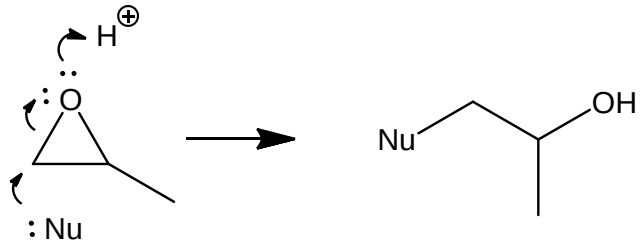

Scheme 1. Epoxide ring opening under acidic pH conditions in the presence of a nucleophile, Nu.

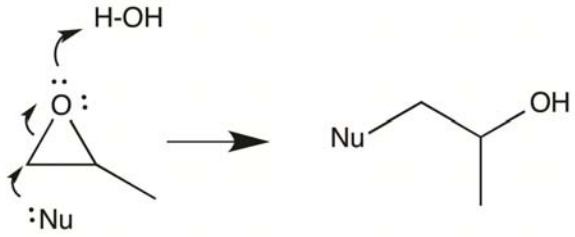

Scheme 2. Epoxide ring opening under basic pH conditions in the presence of a nucleophile, Nu

Under basic conditions, epoxide ring-opening is most likely to occur via a concerted, SN_2 reaction as well. The experimental data shows that the site of attack of the nucleophile is at the least hindered site of the epoxide, which results in the formation of the more substituted alcohol (Scheme 2). If the reaction is purely an SN_2 reaction, a concerted mechanism, then one would expect to see only one degradation product from the ring opening. (10)

Nucleophilicity and reactivity

Nucleophilic attack of the epoxide is common due to the high ring strain of the three-membered ring and the epoxide can react with a large number of nucleophiles, including hydroxide ion (10). The stronger the nucleophile, the more reactive this nucleophile will be and the quicker the epoxide will open (11). Many have tried to quantify the nucleophilicity, starting with the most prominent paper by Swain-Scott in 1953 and work continues in this area today. (12) Swain-Scott studied the reactivity of various nucleophiles, including halides and developed equations to explain the phenomenon (see Equation 1). In the Swain-Scott equation, the rate constant in the presence of the nucleophile (k_n), and the rate constant in water (k^0) yields the electrophilic parameter (s), and the nucleophilic parameter (n). Through these equations, the nucleophilic constants were theorized. Many chemists tried to quantify nucleophilicity and the Swain-Scott equation evolved as more relevant factors were identified. (13)

$$\text{Log } (k_n/k^0) = sn$$

Equation 1: Swain Scott equation

Although it is rare that pure SN_1 and SN_2 reactions occur, the governing reaction pathway can often be identified by the structure and stereochemistry, if the starting epoxide is chiral, of the end products (10).

Catalysis by counter-ions such as halides can also exert a significant effect of the reactivity of epoxides due to competitive addition to the epoxide. Epoxides also undergo nucleophilic attack from other nucleophiles, including amines (10). However, α-keto-epoxides appear to be more stable than standard epoxides due to

the electron withdrawing effect of the α-carbonyl group in the acidic pH range but perhaps more vulnerable to nucleophilic attack under base pH conditions (See Figure 3). (9; 14)

Base catalyzed Isomerization

Under basic pH conditions, there is the possibility of chiral scrambling or epimerization at the C_1 position in some amino acid derivatives. The tertiary carbon at C_1 of PIV-PR-020, a peptide mimetic, can be deprotonated producing a carboanion intermediate, which is resonance stabilized with the enol under basic conditions thereby allowing isomerization (10). Isomerization is a route of peptide degradation (15).

For the PIV-PR-020 molecule, the chiral carbon adjacent to the benzyl group, referred to here as C_1, may form a carboanion intermediate in resonance with the enol form under basic conditions (see Scheme 3). Base can extract the hydrogen atom attached to the chiral carbon and the resulting carboanion is resonance stabilized by the adjacent carbonyl group. (10) When the hydrogen returns, there is no preference in addition, thus resulting in scrambling at the chiral center. The result is a mixture of both diastereomers.

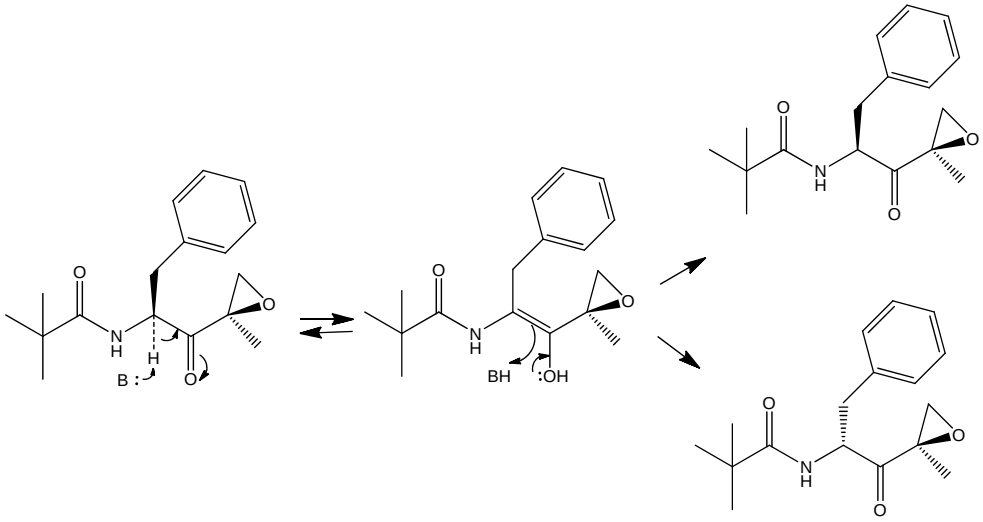

Scheme 3. Proposed base catalyzed isomerization of the chiral carbon at C_1 and the resonance stabilization with the adjacent carbonyl in PIV-PR-020

Specific Aims

The α-keto-epoxide group is present in both the approved drug, carfilzomib, and in the follow on oral drug, oprozomib, as a reactive warhead for proteasome inhibition.

The specific aims of this research were to:

Aim 1- Investigate the degradation kinetics of PIV-PR-020 with the S,R, (S (C_1), R (C_3)) stereochemistry, a model for both carfilzomib and oprozomib, over a pH range of 2 to 8 at various temperatures.

Aim 2 – Elucidate the pathways and possible mechanisms of degradation at the α-keto-epoxide group.

Aim 3- Investigate the reactivity of the α-keto-epoxide in the presence of halide nucleophiles.

EXPERIMENTAL

Materials

PIV-PR-020 with the (S,R), (S(C_1), R (C_3)) stereochemistry where (S,R) refer to (C_1, C_3), the diastereomer, PIV-PR-020 R (C_1), R (C_3), PIV-PR-020 S(C_1), R (C_3) diol, PIV-PR-020 R (C_1), R (C_3) diol, and the PIV-PR-020 S (C_1), R (C_3) chlorohydrin degradation product were synthesized by the Process Chemistry group at Onyx Pharmaceuticals (a subsidiary of Amgen) and the structures were verified by NMR and LCMS. One lot of PIV-PR-020 was used for this study. The synthesis of these materials and the related NMR data and LCMS data are presented in the appendix. The buffers used in the degradation study were prepared from the chemicals listed below. The following chemicals were reagent grade and purchased from VWR (Radnor, PN): sodium chloride (Alfa Aesar, lot 10171522 from Heysham, England), sodium perchloride (Alfa Aesar, lot 10170929 from Heysham, England), Sodium phosphate dibasic pentahydrate Ultrapure (JT Baker, lot 0000023506 from Phillipsburg, NJ), and sodium acetate (Calbiochem, lot VH16D from India), Sodium phosphate monobasic monohydrate Ultrapure (JT Baker, lot 23506 from Center Valley, PA), glacial acetic acid HPLC grade (EMD lot 52312 from Darmstadt, Germany), perchloric acid omnitrace (EMD, Lot 44139, Canada), hydrochloric acid 1N (BDH, lot 1060805, West Chester, PA), sodium bromide (Avantor, lot 0535-02, USA) and sodium iodide hydrate (alfa Aesar, lot A07U042, Ward Hill, MA). Mobile phase buffers were also purchased from VWR, 0.1% formic acid in water (LCMS grade, JT Baker)

and 0.1% formic acid in acetonitrile (LCMS grade, JT Baker). Water for kinetics studies was HPLC grade water from JT Baker.

Preparation of Buffer Solutions and Test Solutions

Each buffer was made up at four times the needed concentration (100mM) and ionic strength was adjusted to 0.6M (four times the needed concentration) using sodium chloride, sodium bromide, sodium iodide and sodium perchlorate, as required. The PIV-PR-020 was prepared at a concentration of 0.667mg/ml in water (1.3 times the needed concentration). The study solutions were prepared by adding one fourth volume of buffer to three fourths volume of PIV-PR-020 solution, thereby making a 0.5mg/ml solution of PIV-PR-020 in 25mM buffer, 0.15 ionic strength. The exact concentration of the solution was determined at time zero by HPLC for all studies. Phosphate buffers of higher or lower concentrations were prepared in the similar fashion.

pH Measurements

The pH measurements were performed at ambient conditions using a Thermo Orion 9863BN needle tip combination electrode. The electrode was calibrated with a three point standards bracketing the intended pH range before each series of measurements. The pH values of buffers can change with respect to temperature, therefore all buffers prepared at ambient condition take into account any shifts in pH due to temperature.

High Performance Liquid Chromatography (HPLC) Analysis

An Agilent 1290 (Palo Alto, CA) High Pressure Liquid Chromatography—Ultraviolet Spectroscopy (HPLC—UV) instrument equipped with a G4220A Infinity binary pump, G4212A Infinity DAD detector, G1316C thermostat column compartment, G4226A Infinity auto sampler, and 2.1 x 50 mm 1.8 μm Zorbax Eclipse C18 Column were used for the analysis. Elution was performed using a solvent gradient of 20% to 60% B (B = 0.1% formic acid in acetonitrile) in solvent A (A = 0.1% formic acid in water) for 25 minutes at a flow rate of 1 mL/min. Column temperature was maintained at 10°C ±0.5°C to ensure peak separation. Peaks were detected and adequately separated at 220 nm and Agilent OpenLab analysis software was used to integrate peak area.

High Performance Liquid Chromatography Mass Spectroscopy (HPLC-MS) Analysis

An Agilent 1290 (Palo Alto, CA) High Pressure Liquid Chromatography—Ultraviolet Spectroscopy (HPLC—UV) instrument equipped with a Agilent 6150 quadropole LC/MS, G4220B Infinity binary pump, G4212A Infinity DAD detector, G1316C thermostat column compartment, G4226A Infinity binary pump, Infinity auto sampler, and 2.1 x 50 mm 1.8 μm Zorbax Eclipse C18 Column were used for the analysis. Elution was performed using a solvent gradient of 20% to 60% B (B = 0.1% formic acid in acetonitrile) in solvent A (A = 0.1% formic acid in water) for 25 minutes at a flow rate of 1

mL/min. Column temperature was maintained at 10°C ±0.5°C to ensure peak separation. Peaks were detected and adequately separated at 220 nm and Agilent OpenLab analysis software was used to integrate peak area and the peak mass. The degradation peaks were adequately separated by this method at a UV absorbance of 220nm across all pH values.

Preparation of samples for NMR Verification

Samples of PIV-PR-0020, PIV-PR-020 (R,R) diastereomer, PIV-PR-020 (S,R) diol, PIV-PR-020 (R,R) diol, and the PIV-PR-020 (S,R) chlorohydrin, which were synthesized by the Process Chemistry group at Onyx Pharmaceuticals (a subsidiary of Amgen) were sent to Acorn NMR Inc. (Livermore, CA) for ^{13}C and proton NMR analysis to confirm the chemical structure. All NMR spectra are presented in the appendix.

Kinetic Studies

pH stability studies at 25ºC

Kinetic studies at pH values of 2, 4, 5, 7, and 8 were carried out at 25ºC in an aqueous buffers at constant ionic strength, I = 0.15 (NaCl). Reactions were initiated by mixing one in four volumes of aqueous buffer solution with an PIV-PR-020 aqueous solution at 25 ºC. The final concentration of PIV-PR-020 in the reaction mixtures was 1.4-1.6 x 10^{-3} M measured by HPLC, and the buffer concentration was 25mM. After initiation, the pH_{app} was measured and aliquots of the reaction mixture were transferred to HPLC vials and incubated in a

temperature controlled incubator at 25ºC. At appropriate time points, samples were pulled and placed in a thermostated HPLC sample holder at 25ºC just prior to injection. Similar studies were carried out at 40°C and 60°C except the vials were stored at the higher temperatures.

Effect of buffer concentration at 25ºC

Kinetic studies with varying phosphate buffer concentrations of 12.5mM, 25mM, and 50mM were evaluated at 25°C at constant ionic strength, I = 0.15 (NaCl).

Effect of halides at 25ºC

Kinetic studies with varying halides at pH 2 were evaluated at 25°C at constant ionic strength, I = 0.15 using sodium chloride, sodium bromide, sodium iodide, and sodium perchlorate. Reactions were initiated by mixing one in four volumes of aqueous buffer solution in PIV-PR-020 aqueous solution. The final concentration of PIV-PR-020 in the reaction mixtures was 1.4-1.6 x 10^{-3} M. After initiation, the pH_{app} was measured samples were stored in a 25°C incubator. Aliquots of the reaction mixture transferred to HPLC vials and the pH was measured right before injection. Test solutions containing sodium iodide were kept in amber glass bottles and HPLC vials to protect from light.

Effect of chloride concentration at 25ºC

Kinetic studies with varying chloride concentrations from 0.04M to 1.5M at pH 2 were evaluated at 25°C at ionic strength, I = 0.15 using sodium chloride, or sodium perchlorate (with the exception of the 10x NaCl solution). Reactions were initiated by mixing one in four volumes of aqueous buffer solution in PIV-

PR-020 aqueous solution. After initiation, the pH_{app} was measured samples were stored in a 25°C incubator. Aliquots of the reaction mixture transferred to HPLC vials and the pH was measured right before injection.

All kinetic studies were carried out to three half-lives and the rate order was determined by fitting the data in to a zero-order, first-order and second-order plot. In addition, representative degraded samples were run on the LCMS and the degradation main peaks were identified by comparing to four known degradation products.

Generation of Standard Curves

A standard curve for PIV-PR-020 was generated by weighing out two samples of 5mg of PIV-PR-020 into a 25ml volumetric flask and adding one to one by volume of acetonitrile and water to the flask for a total concentration of 0.2mg/ml PIV-PR-020. A serial dilution to obtain a concentration range of 0.2mg/ml and 0.02mg/ml was performed and analyzed by HPLC to generate a three point standard curve. The concentration of PIV-PR-020 was plotted against the HPLC area to produce a linear standard curve. The other 0.2mg/ml standard of was used as a check for the standard curve to ensure no error in weighing. Chromatograms showed only the presence of PIV-PR-020 in freshly prepared samples.

RESULTS

Determination of Rate Constants

The loss of PIV-PR-020 with time in aqueous solution (I = 0.15 adjusted with NaCl) at 25°C were determined at pH values of 2, 4, 5, 7 and 8, by monitoring the loss of the parent peak over the course of two to three half lives by HPLC. The observed rate constants were calculated from the slope of the curve of Ln[D] vs. time (min) using the first order rate equation, where Ln represents the natural logarithm and [D] is the concentration of molecule, PIV-PR-020. First-order rate constants were calculated from the slopes. The various plots shown in Figure 4 illustrate the loss of PIV-PR-020 followed apparent first order kinetics for most of the pH values in this study. The data at pH 8 showed some deviation from first order kinetics and this will be discussed later.

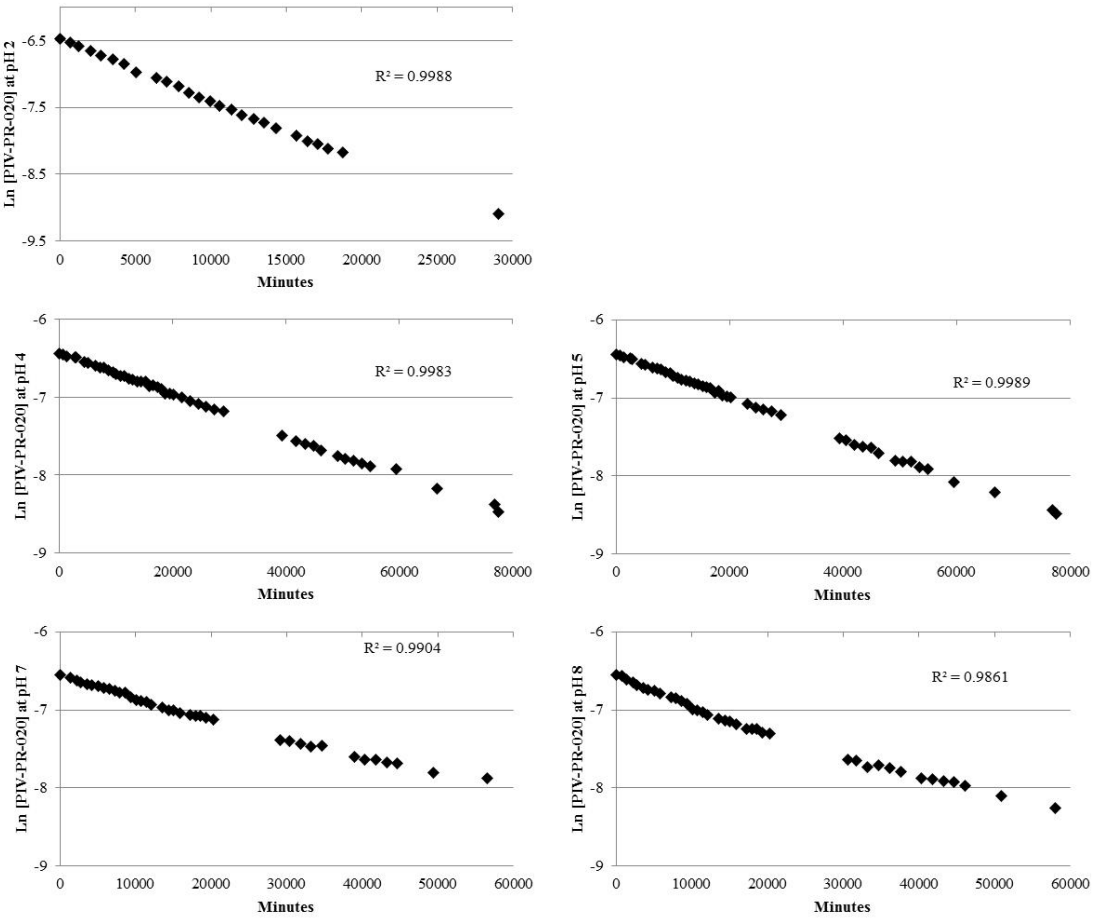

Figure 4. Plots of the natural logarithim of PIV-PR-020 remaining versus time at pH values 2, 4, 5, 7, and 8, respectively. Data for 25°C at 0.15 ionic strength adjusted with NaCl.

The main degradation peaks of PIV-PR-020 were also monitored over the course of the reaction. The degradation products previously proposed and synthesized were also followed; PIV-PR-020 (R,R) diastereomer, PIV-PR-020 (S,R) diol, PIV-PR-020 (R,R) diol, and the PIV-PR-020 (S,R) chlorohydrin (see Figure 5). Additional peaks seen in the chromatograms were also followed and noted by their relative retention times. The LCMS of the four proposed degradation standards determined is shown in the appendix and their molecular

weights, the relative retention times, and retention times determined by HPLC are shown in Table 1.

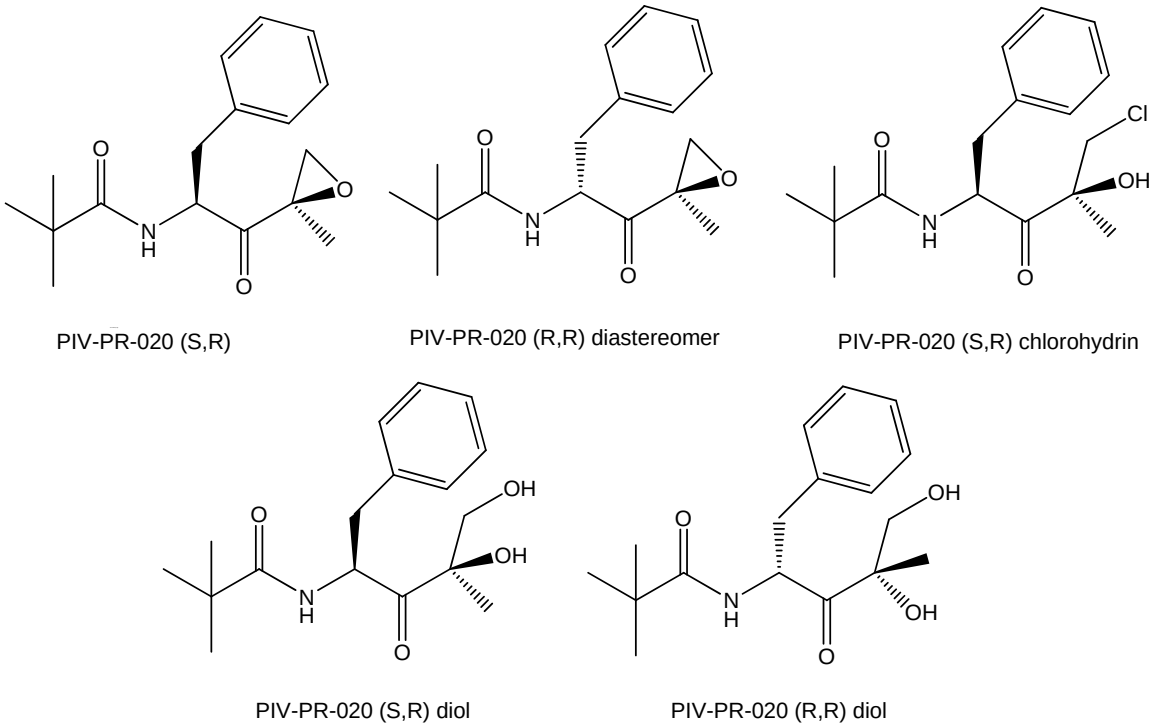

Figure 5. Structures of PIV-PR-020 with the (S,R) stereochemistry and its proposed degradation products (as standards), PIV-PR-020 (R,R) diastereomer, PIV-PR-020 (S,R) chlorohydrin, PIV-PR-020 (S,R) diol, and the PIV-PR-020 (R,R) diol..

	PIV-PR-020	PIV-PR-020 (R,R) diastereomer	PIV-PR-020 (S,R) chlorohydrin	PIV-PR-020 (S,R) diol	PIV-PR-020 (R,R) diol
RT (min)	17.1	14.1	16.8	10.4	8.9
RRT	1	0.82	0.98	0.61	0.52
MW	289	289	325	307	307

Table 1. Table showing the retention times (RT), relative retention times (RRT) and molecular weight (MW) of PIV-PR-020 and the four proposed or expected degradation products, as standards, PIV-PR-020 (R,R) diastereomer, PIV-PR-020 (S,R) chlorohydrin, PIV-PR-020 (S,R) diol, and the PIV-PR-020 (R,R) diol..

Appearance of Degradation Peaks

In addition to the kinetics of disappearance of PIV-PR-020, the main degradation products were monitored over the course of the study by HPLC at 220nm. Peak areas were plotted versus time at all pH values (Figures 6 through 10). Assuming the same response factor for the known and unknown degradation products over the pH range of 2 to 7, there is good mass balance over the course of the study. At pH 8, however, mass balance was not observed with greater than 25% degradation. At pH 8 there is relatively good mass balance, about 91%, for the first 25% of the reaction and 81% for the first 50% of the reaction.

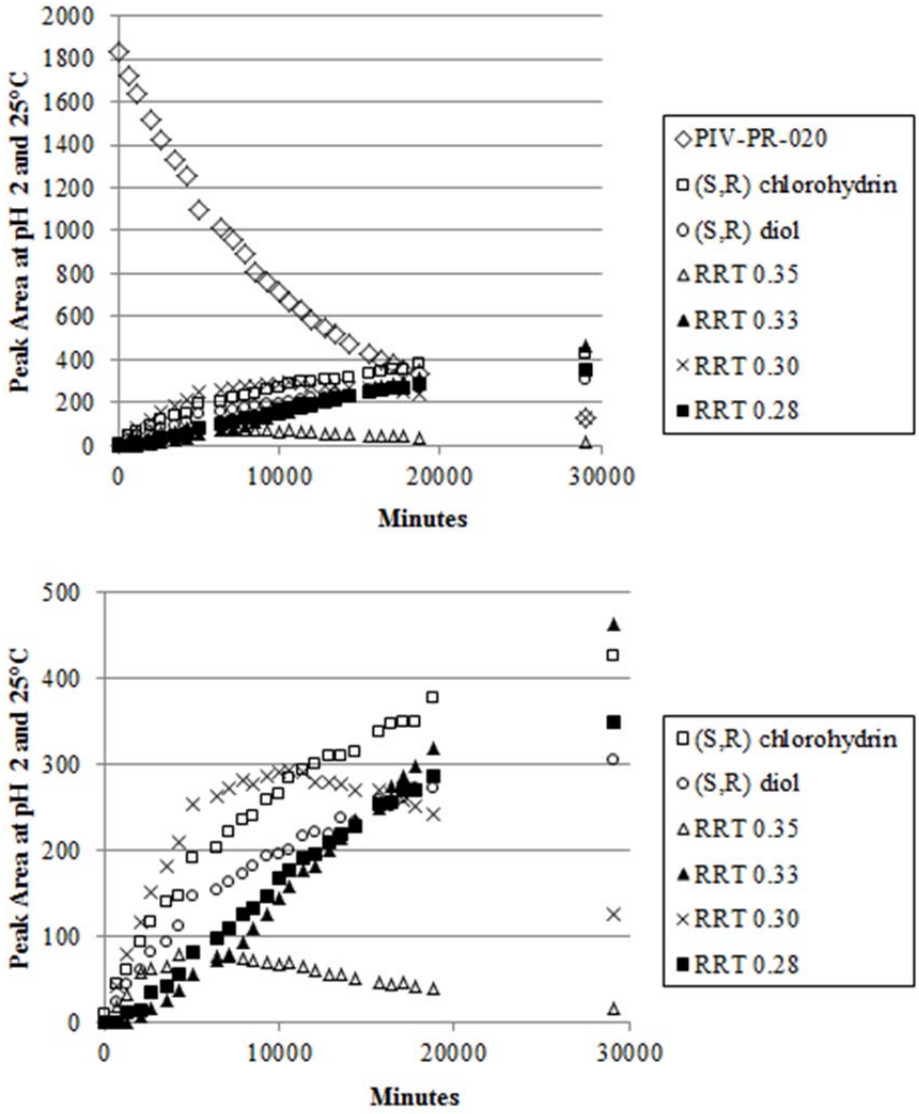

Figure 6. Plots showing the loss of PIV-PR-020 and the formation of the degradation products in the upper figure and the lower figure shows only the appearance of the degradation products; (S,R) chlorohydrin, (S,R) diol, and the 4 peaks with an apparent MW of 307 (0.35, 0.33, 0.30, and 0.28 RRT) at pH 2, at 25°C and *I* = 0.15 (NaCl).

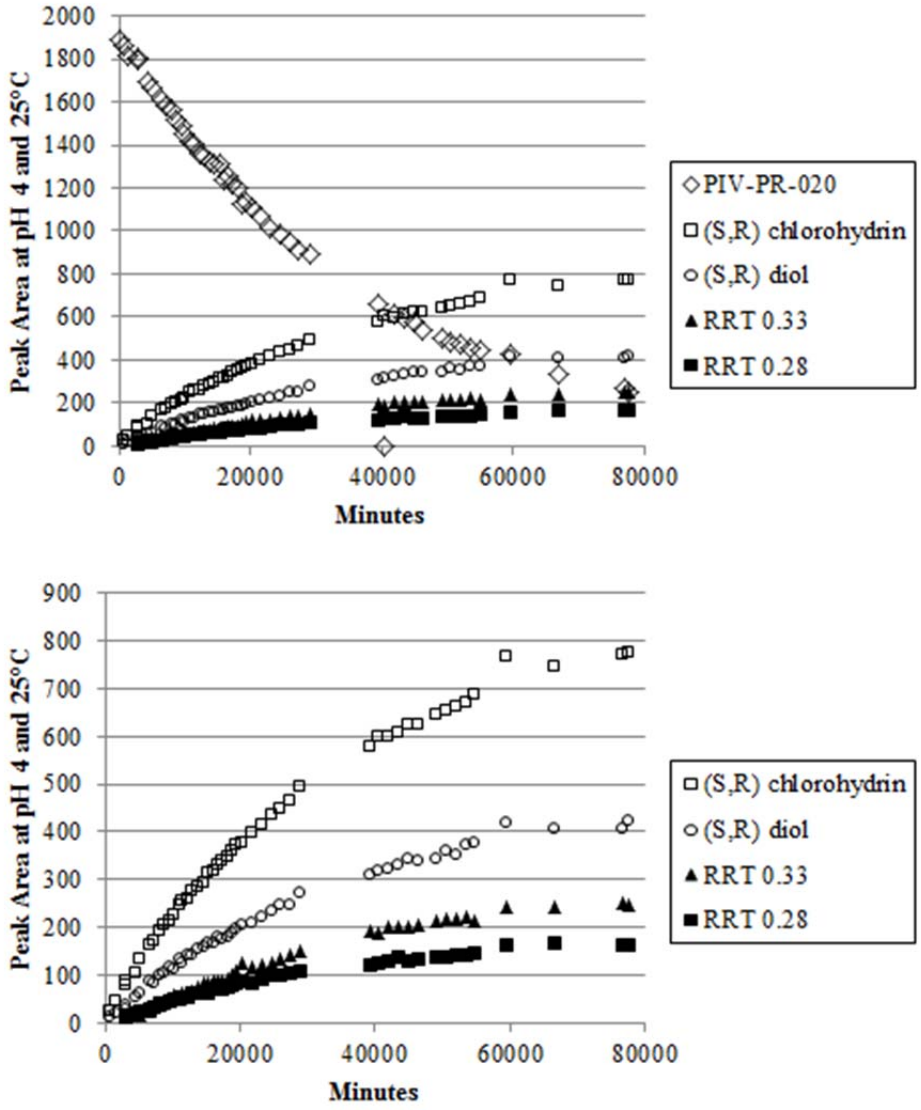

Figure 7. Plots showing the loss of PIV-PR-020 and the formation of the degradation products in the upper figure and the lower figure shows only the appearance of the degradation products; (S,R) chlorohydrin, (S,R) diol, and the 2 peaks with an apparent MW of 307 (0.33, and 0.28 RRT) at pH 4, at 25°C and *I* = 0.15 (NaCl).

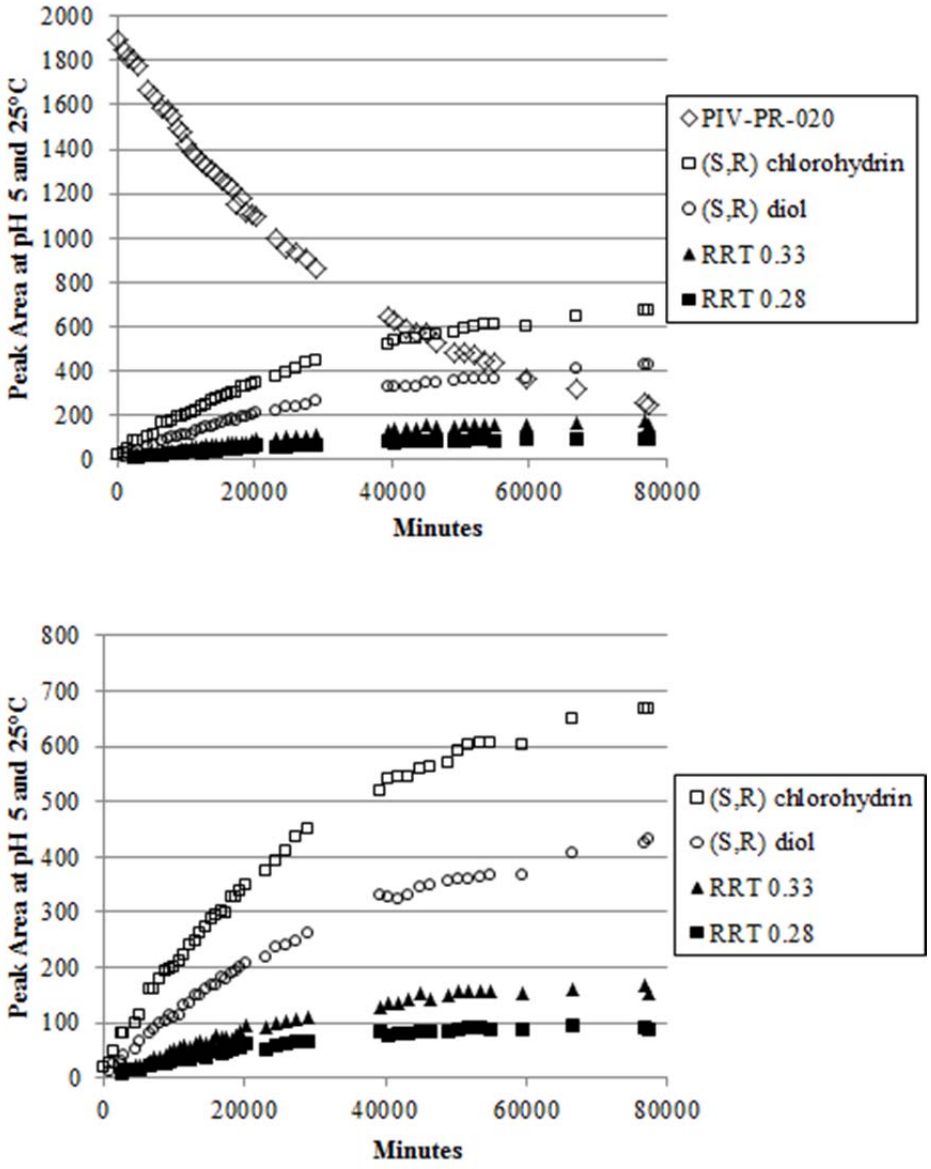

Figure 8. Plots showing the loss of PIV-PR-020 and the formation of the degradation products in the upper figure and the lower figure shows only the appearance of the degradation products; (S,R) chlorohydrin, (S,R) diol, and the 2 peaks with an apparent MW of 307 (0.33, and 0.28 RRT) at pH 5, at 25°C and *I* = 0.15 (NaCl).

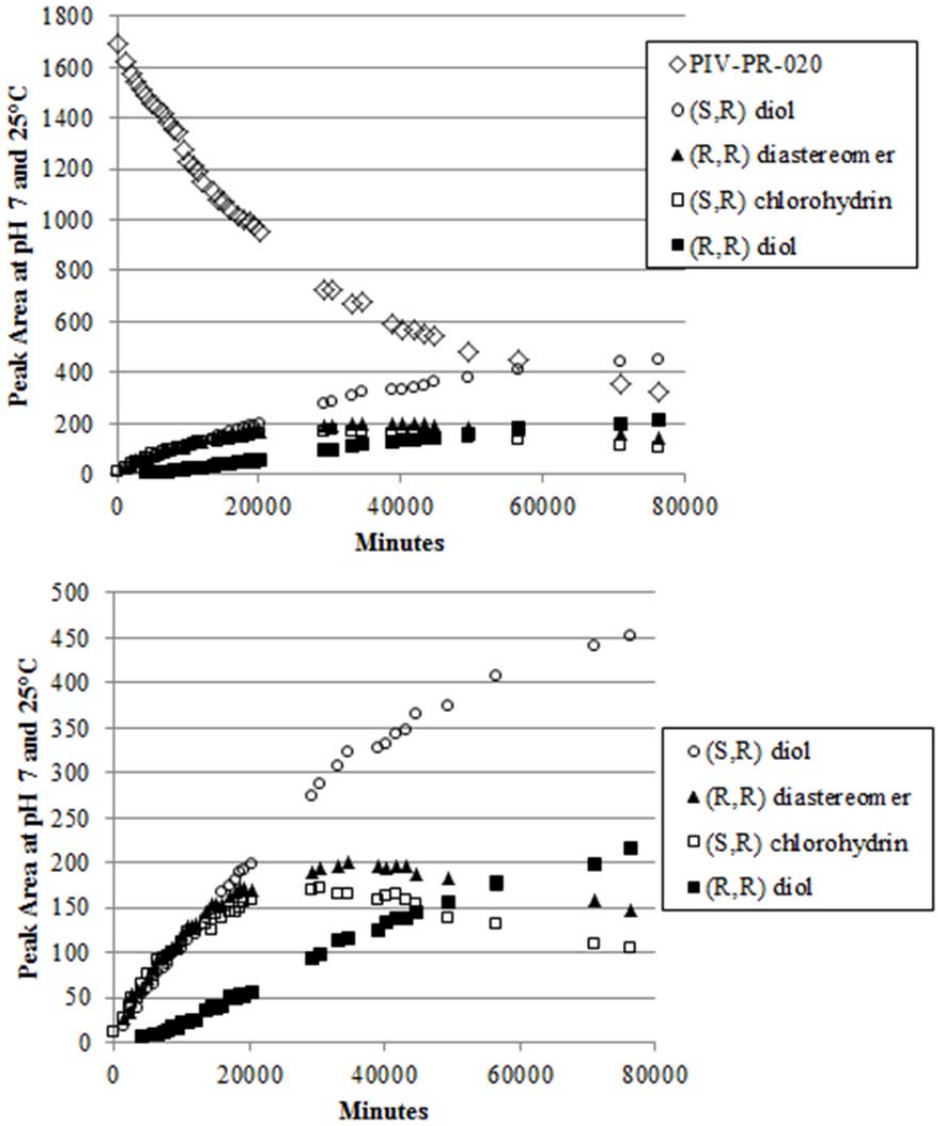

Figure 9. Plots showing the loss of PIV-PR-020 and the formation of the degradation products in the upper figure and the lower figure shows only the appearance of the degradation products; (S,R) diol, (R,R) diastereomer, the (S,R) chlorhydrin, and the (R,R) diol at pH 7, at 25°C and *I* = 0.15 (NaCl).

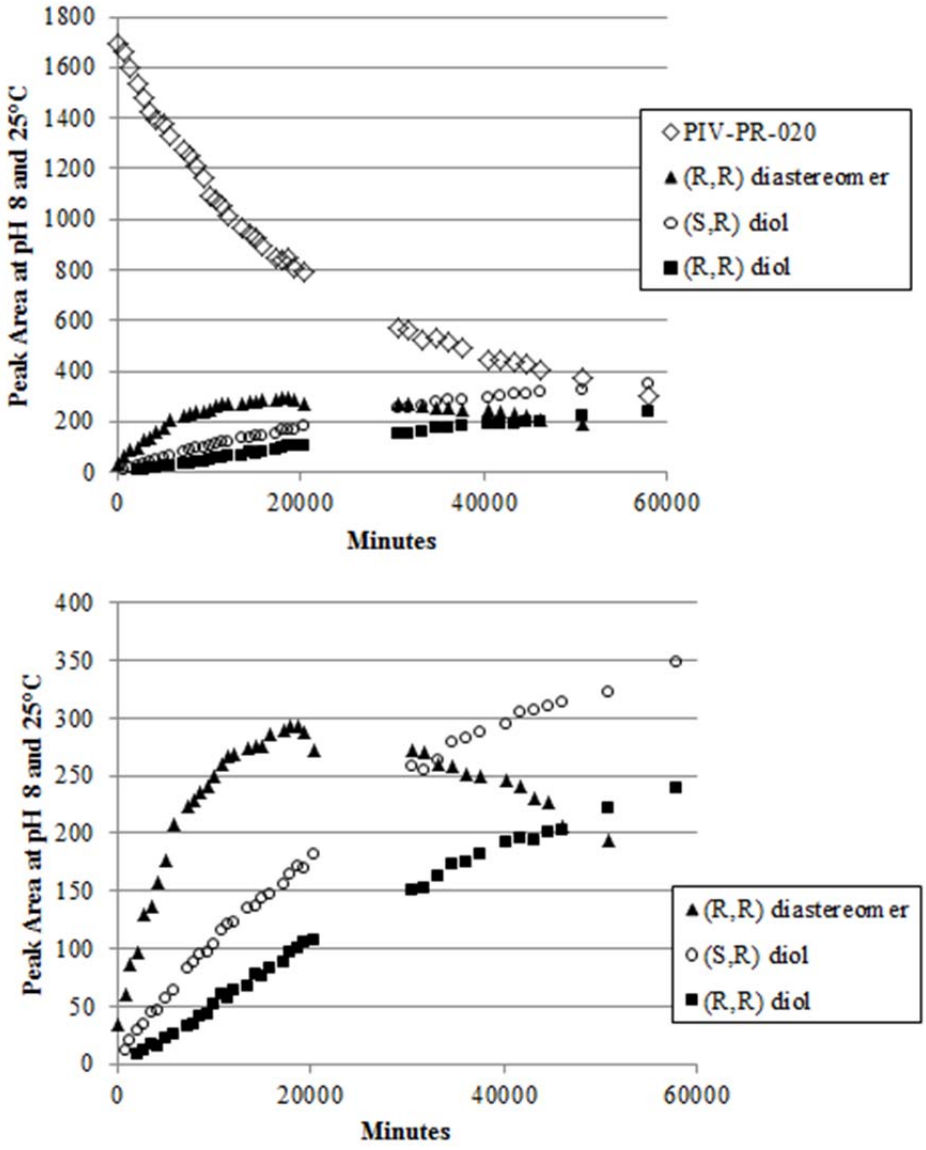

Figure 10. Plots showing the loss of PIV-PR-020 and the formation of the degradation products in the upper figure and the lower figure shows only the appearance of the degradation products; (R,R) diastereomer, (S,R) diol and (R,R) diol at pH 8, at 25°C and *I* = 0.15 (NaCl).

The Effect of Temperature

The kinetics of loss of PIV-PR-020 in aqueous solution (were also determined at 40°C and 60°C at pH values of 2, 4, 5, 7 and 8, over the course of two to three half lives by HPLC. Observed first-order rate constants were calculated as described for the 25°C data. An Arrhenius plot for the data collected at pH 4 is shown in Figure 11, and the calculated activation energies are for all pH values are in Table 2.

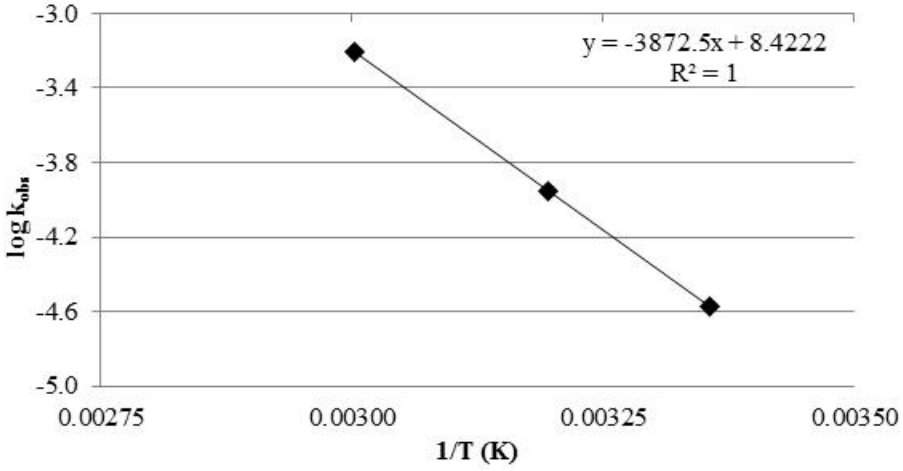

Figure 11. Arrhenius plot for the degration of PIV-PR-020 at pH 4 in acetate buffer

	PIV-PR-020 pH 2	PIV-PR-020 pH 4	PIV-PR-020 pH 5	PIV-PR-020 pH 7	PIV-PR-020 pH 8
Ea (kcal/mol)	16.8 ± 0.1	17.7 ± 0.0	17.8 ± 0.0	18.6 ± 0.1	20.3 ± 0.1

Table 2. Calculated activation energies of PIV-PR-020 at pH values 2, 4, 5, 7, and 8 from Arrhenius plots.

The Effect of Varying pH on the Loss of PIV-PR-020

The pH-rate profile at 40°C was identified by plotting the logarithm of the observed rate constants against pH (see Figure 12). The pH rate profile for all other temperatures and observed rate constants are presented in the appendix.

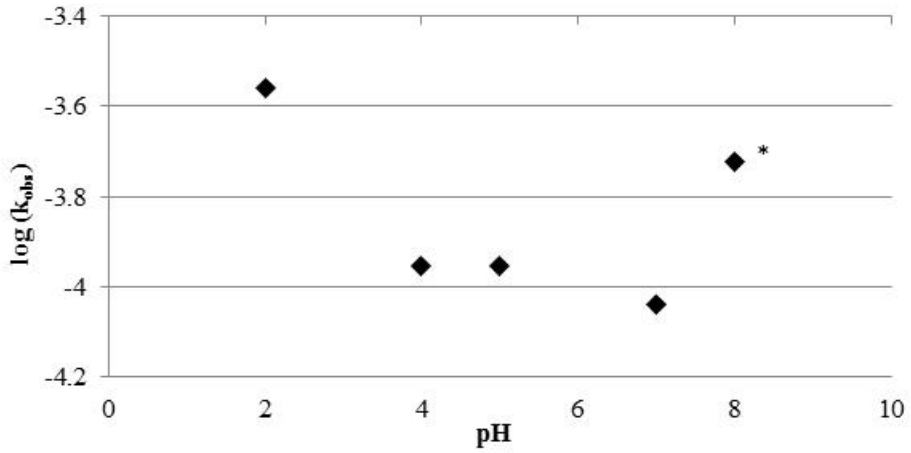

Figure 12. pH-rate profile for the degradation of PIV-PR-020 at 40°C in aqueous buffers with the ionic strenght adjusted with sodium chloride.

*** pH 8 value is an approximation since it does not follow pure first order kinetics throughout the full time course of the study.**

Buffer Concentration Effects

The loss of PIV-PR-020 in aqueous solution at 25°C and ionic strength adjust to 0.15 with sodium chloride at pH 8 in sodium phosphate buffer concentrations of 12.5mM to 50mM were monitored over the course of two to three half lives by HPLC. The plots are shown in Figure 13 and the observed rate constants are listed in Table 3.

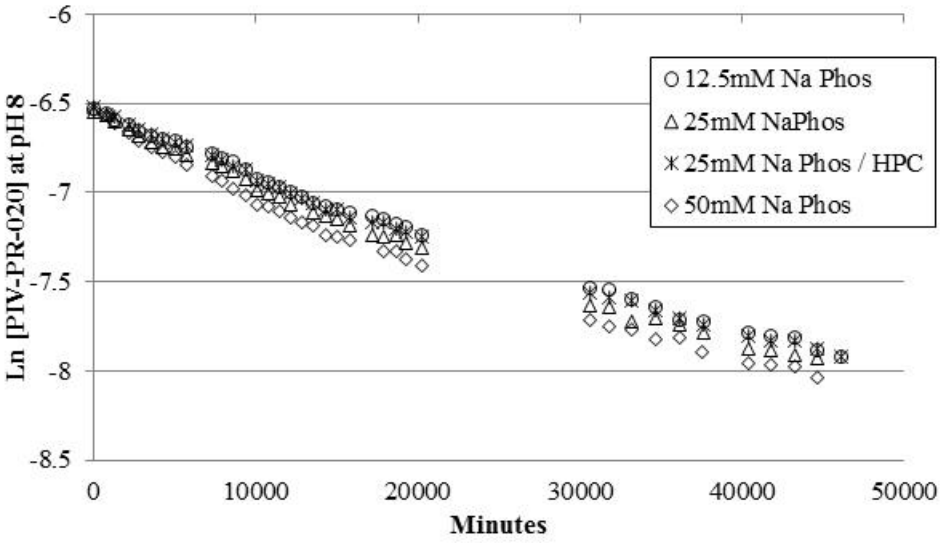

Figure 13. Plots of the natural logarithim of PIV-PR-020 remaining versus time at pH 8 at 25°C in the presence of varying phosphate buffer concentrations ranging from 12.5mM to 50mM.

Buffer	Sodium Phosphate 0.0125M	Sodium Phosphate 0.025M	Sodium Phosphate 0.025M	Sodium Phosphate 0.050M
Salt	NaCl	$NaClO_4$	NaCl	NaCl
k_{obs} (min^{-1})	2.98×10^{-5}	3.02×10^{-5}	3.14×10^{-5}	3.26×10^{-5}

Table 3. Observed first-order rate constant, k_{obs}, values for loss of PIV-PR-020 at pH 8 with varying sodium phosphate buffer concentrations of 0.0125M, 0.025M, and 0.50M, and 1.5M by HPLC at 25°C.

Chloride Ion Concentration Effects at pH 2

The loss of PIV-PR-020 in aqueous solution at 25°C and pH 2 with theoretical chloride concentrations of 0.04M (I = 0.15 adjusted with $NaClO_4$, but said to contain up to 2.5% NaCl), 0.15M (I = 0.15 adjusted with NaCl), and 1.5M (I = 1.5 adjusted with NaCl). The reaction rates were monitored over the course of two to three half lives by HPLC. The observed rate constants were calculated from the slope of the curve of Ln[D] vs. time (min) using first order rate equation

(shown in Figure 14). Observed first-order rate constants were calculated as the slopes of the semi logarithmic plots of the HPLC area at 220nm (Table 4).

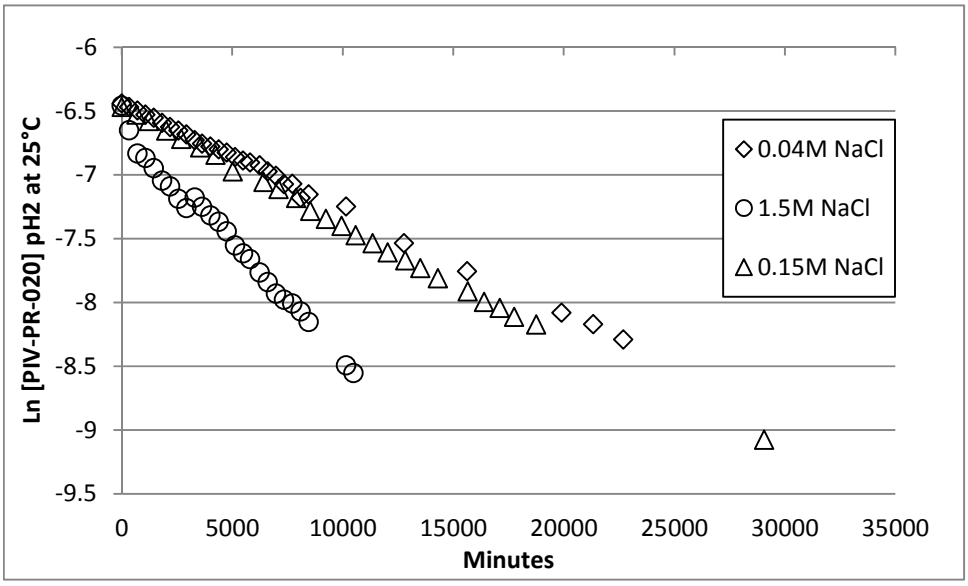

Figure 14. Plot of Ln[D] vs time for PIV-PR-020 at pH 2 at 25°C in the presence of chloride concentration ranging from 0.04M to 1.5M.

Salt	Low NaCl 0.04M	Mid NaCl O.15 M	High NaCl 1.5 M
k_{obs} (min^{-1})	8.22×10^{-5}	9.13×10^{-5}	1.81×10^{-4}

Table 4. Observed first-order rate constant values, k_{obs}, for loss of PIV-PR-020 at pH 2 at various chloride concentrations of 0.04M, 0.15M, and 1.5M by HPLC at 25°C.

Halide Effect

The loss of PIV-PR-020 in aqueous solution at 25°C and pH 2 with I = 0.15 using sodium perchlorate, sodium chloride, sodium bromide, and sodium iodide was followed by monitoring the loss of parent peak over two to three half

lives by HPLC. The observed rate constants were calculated from the slope of the curve of Ln[D] versus time (min) using first order rate equation. The observed first-order rate constants are listed in Table 5. A plot of log (k_{obs}) against the Swain-Scott nucleophilic number, n, is shown in Figure 15.

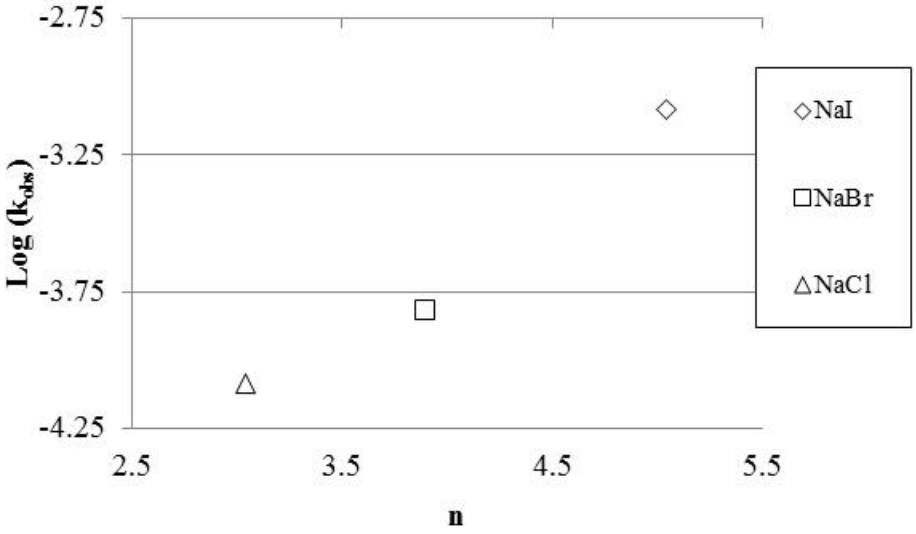

Figure 15. A Swain-Scott plot of the logarithmic of the first order rate constants, k_{obs} versus the nucleophilic reactivity parameter for the losss of PIV-PR-020 at pH 2 with various halide nucleophiles (chloride, bromide, and iodide) by HPLC at 25°C *I* = 0.15 with NaCl, NaBr or NaI.

Salt	NaCl	NaBr	NaI
k_{obs}	8.22×10^{-5}	1.52×10^{-4}	8.28×10^{-4}

Table 5. Observed first-order rate constant, k_{obs}, values for loss of PIV-PR-020 at pH 2 with various halide nucleophiles (chloride, bromide, and iodide) by HPLC at 25°C *I* = 0.15.

DISCUSSION

Loss of PIV-PR-020 as a function of pH and temperature

The overall loss of PIV-PR-020 follows approximate first order kinetics under most conditions. The k_{obs} for each pH value at each temperature were identified from the slopes of the semi logarithmic plots of the loss of PIV-PR-020 versus time. The major degradation pathways are summarized in scheme 4 as a function of pH (at pH values 2, 4, 5, 7, and 8). For each temperature studied the k_{obs} are plotted versus pH to obtain a pH-rate profile. This profile (in general) follows the expected U-shaped pH rate profile for the degradation of an unionizable compound such as PIV-PR-020. Because of the limited number of data points no effort was made to fit the profile to Equation 2 below.

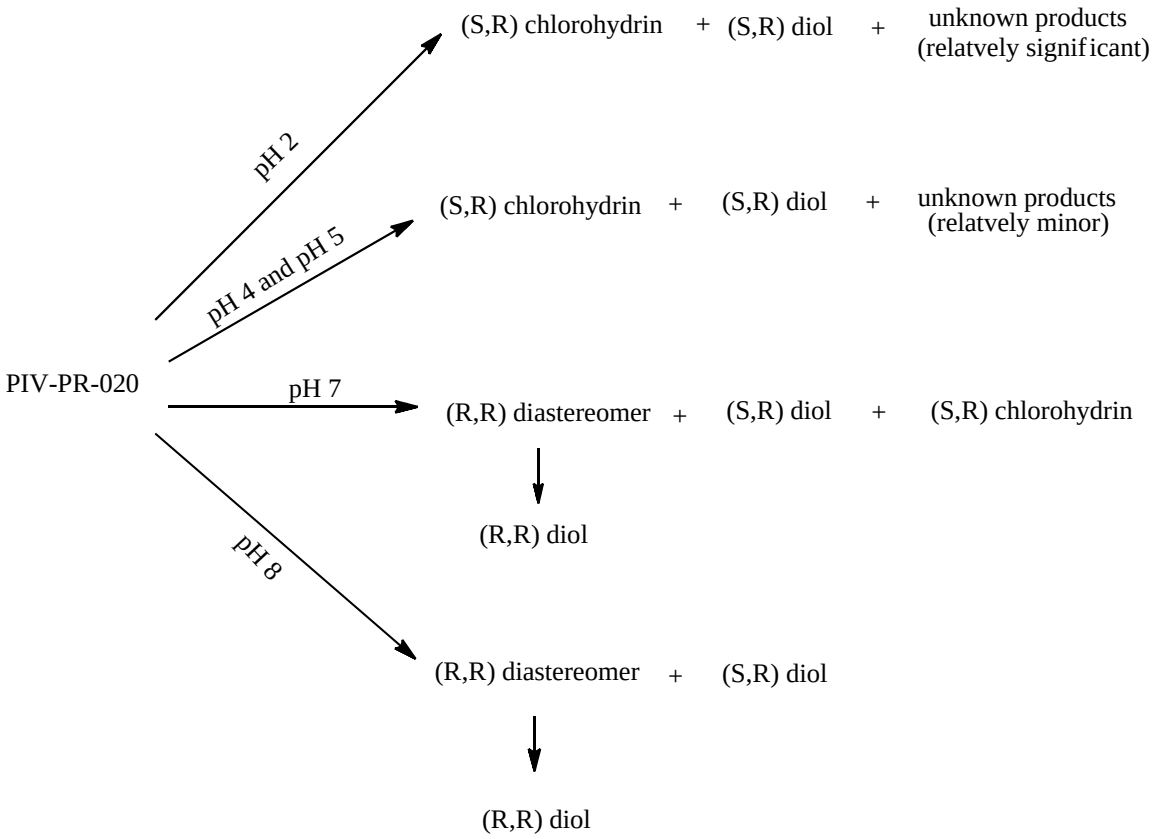

Scheme 4. Basic reaction scheme for the loss of PIV-PR-020 at different pH values

The reaction is largely pH independent except at pH values below 4 and above 7 such that it can be defined by the equation 2. Where k_w is the rate constant at in the pH range of 4-8. k_H is the acid catalyzed rate constant and k_{OH} is the base catalyzed rate constant.

$$k_{obs} = k_W + k_H[H+] + k_{OH}[OH-]$$

Equation 2: Rate equation

At pH values below 7, the main degradation products of the warhead in the presence of sodium chloride are the (S,R) chlorohydrin and (S,R) diol. As noted earlier there are an additional four peaks eluding early in the chromatogram

(0.28RRT, 0.30RRT, 0.33RRT, and 0.35RRT) with the same apparent molecular weight as the diol of unknown structure.

A typical chromatogram for the reaction at pH 2 is shown in Figure 16 accompanied by a typical LCMS chromatogram in Figure 17. It clearly indicates that PIV-PR-020, (S,R) chlorohydrin at 16.8 min (0.98RRT), (S,R) diol at 10.3 min (0.61RRT) and all other degradation peaks can be separated from one another. The four additional peaks at the early retention times in the low pH chromatogram have the same apparent molecular weight as the diol by LCMS. When a degraded pH 2 sample with these four early eluding peaks is pH adjusted up to pH 7, two of these peaks (0.30RRT and 0.35RRT) are no longer present and the other two peaks at 0.28RRT and 0.33RRT have slightly higher areas. More work is needed to elucidate the structure and the reaction mechanisms of these four early eluding degradation products.

For oprozomib, the formation of a gem diol has been suggested, but the structure is not very stable. (1) Since these diols are not part of the warhead per se and are difficult to make, isolate, and evaluate, they were not considered in this study.

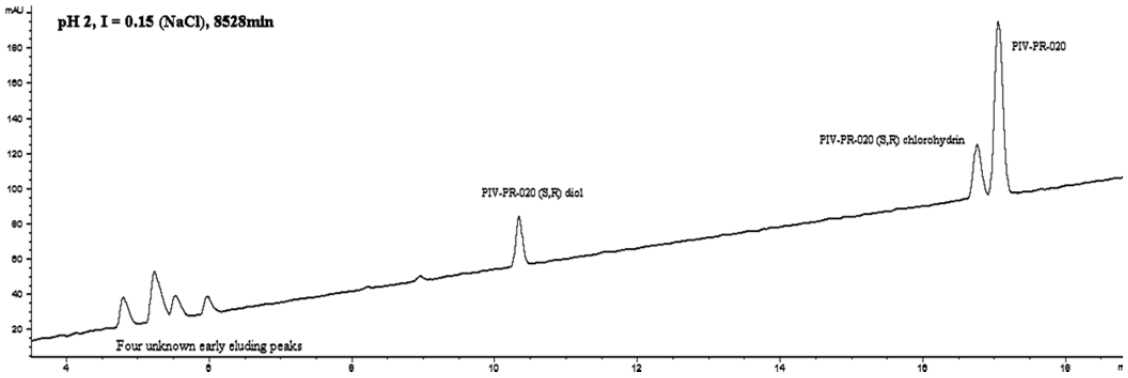

Figure 16. Representative HPLC chromatogram from the loss of PIV-PR-020, at pH 2 in the presence of chloride ions.

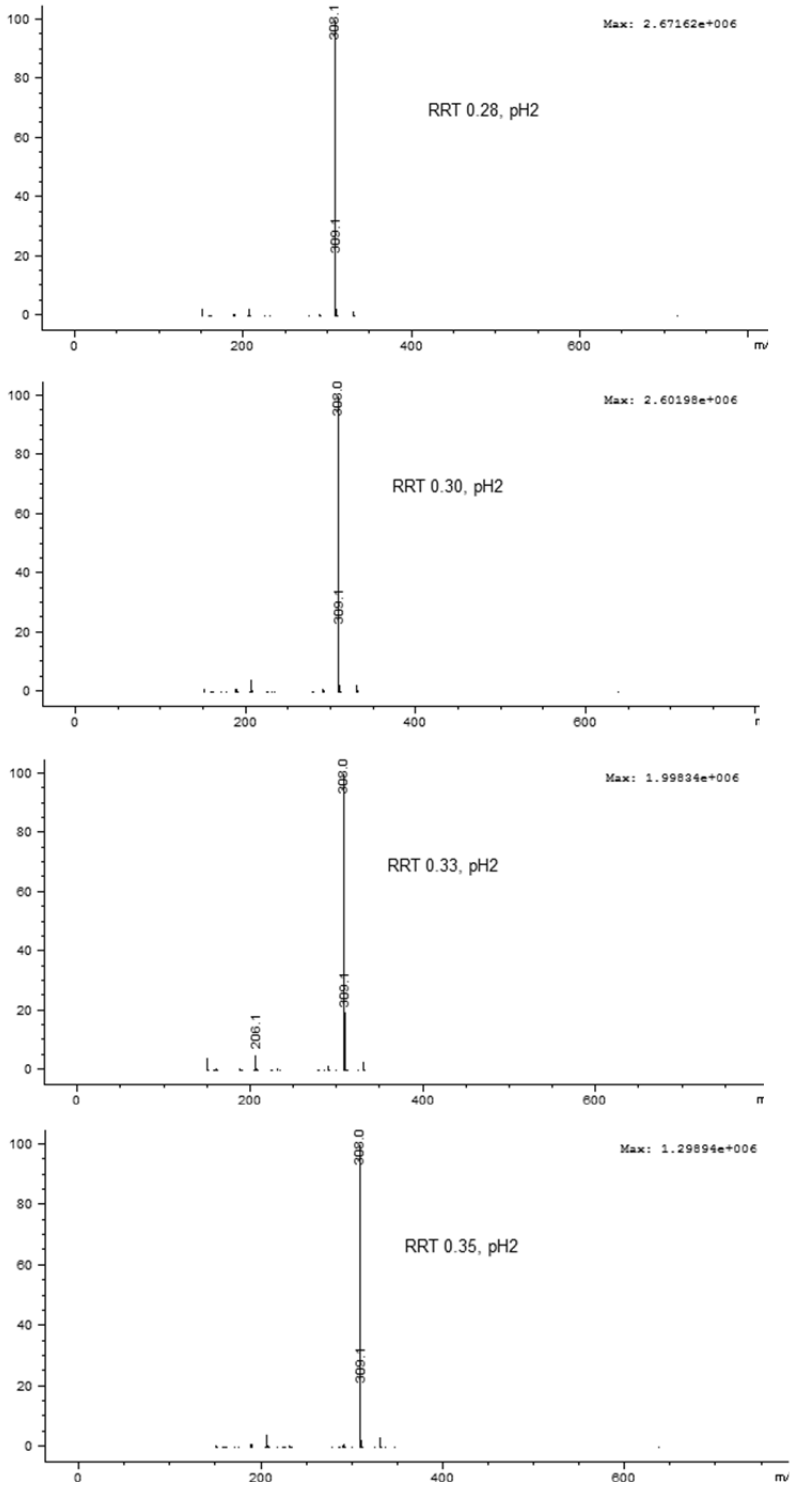

Figure 17. Representative LCMS chromatogram of the degradation products of PIV-PR-020 at pH 2 at 25°C at 13515 minutes, the early eluding degradation products (0.28RRT, 0.30RRT, 0.33RRT, and 0.35RRT).

At pH values 4 and 5, the two main degradation products are the (S,R) chlorohydrin and (S,R) diol. However, as the pH values increase from pH 2 to pH 4 to pH 5, (S,R) diol formation begins to increase relative to the (S,R) chlorohydrin and the four early eluding peaks, specifically the 0.35RRT and 0.30RRT peaks, which decrease. At pH 7 these early eluding peaks are not seen. If there is no chloride ion present, as expected, no chlorohydrin formed.

At pH 7, the main identifiable degradation product is (S,R) diol and some (S,R) chlorohydrin. In addition, the (R,R) diastereomer, and (R,R) diol, are seen. The degradation profile at pH values of 7 and 8 show that (R,R) diastereomer is the primary initial degradation product.

At pH 8, the main degradation product detected by HPLC at 220nm is the (R,R) diastereomer as confirmed from LCMS analysis and the use of the synthesized standard, indicating the main reaction is a based catalyzed isomerization at the C_1 chiral carbon. Over the course of the study there is a loss of the (R,R) diastereomer indicating the (R,R) diastereomer product further degrades. Both (S,R) diol and (R,R) diol form, however (R,R) diol has an appearance lag-time indicating this is possibly the secondary degradation product being formed from (R,R) diastereomer.

There is significant loss in mass balance over the course of the reaction at pH 8 as noted earlier on long-term degradation but over the first 25% of the degradation, based on peak area analysis, 94% mass balance can be accounted for by the known degradation products.

As expected, increased temperature increases the rate of decomposition. It is also important to note that as the temperature increases, the degradation products do not change at any given pH, and therefore do not affect the overall degradation pathway. This would indicate that all reactions have similar energies of activation. Using the Arrhenius Equation for the reaction at pH 4, see Figure 11, the apparent activation energy for the reactions was calculated to be 17.7 kcal/mole but increased in value in going from pH 2 to pH 8, consistent with different pathways becoming more or less important with the pH changes.

Loss of PIV-PR-020 as a function of Buffer Concentration at pH 8

As sodium phosphate buffer was varied (12.5mM, 25mM, and 50mM) at pH 8 and 0.15 ionic strength using sodium chloride, the degradation rate was experimentally determined and the degradation profiles were compared. Chromatograms for the loss of PIV-PR-020 in the presence of increasing phosphate showed no additional product peaks (including any obvious perturbations at the solvent front) (data not shown). The rates of loss of PIV-PR-020 for all the buffer strengths were within 5% and therefore there is minimal buffer strength effect on the degradation of PIV-PR-020. The rate of both (S,R) diol and (R,R) diol is unaffected by buffer concentration. However amount of (R,R) diastereomer increases with increasing buffer strength by 12 to 17 percent and the rate of formation increases slightly.

Loss of PIV-PR-020 as a function of Chloride Concentration at pH 2

Increasing the ionic strength by the addition of sodium chloride from 0.04M, to 0.15M to 1.5M did have a significant effect on the reaction rate at pH 2. The trace chloride content, 0.04M, represents the chloride content using 0.15M sodium perchlorate. Since the ionic strengths of the solutions were kept constant (with the exception of 1.5M sodium chloride), this secondary salt effect appears significant.

Loss of PIV-PR-020 as a function of Halide Effect at pH 2

At pH 2, the degradation rates were experimentally determined as a function of halide nucleophilicity at a constant ionic strength of 0.15 using sodium perchlorate, sodium iodide, sodium bromide, and sodium chloride. The lot of sodium perchlorate which was used during this study did have a small amount of sodium chloride present, about 2.5% by weight. Chloride ion is a less reactive (not as nucleophilic) as bromide or iodide. Each of the halides react with PIV-PR-020 to form their respective PIV-PR-020 halohydrin product. The iodine has a significant impact on the reaction rate and heavily weights the plot. The relative rate in which the halide ion reacts to replace the substituent is a term called the relative reactivity or nucleophilicity of the ion. The k_{obs} of each counter-ion was calculated and plotted against the nucleophilic reactivity parameter of each halide nucleophile to determine if nucleophilicity of the halide has an impact on the rate of degradation at low pH values. According to Figure

15, the reaction rate constant showed a log-linear relationship to the nucleophilic parameter.

CONCLUSIONS

The degradation rate profile of PIV-PR-020 was used as a model for the more structurally complex drugs, oprozomib and carfilzomib. The loss of PIV-PR-020 followed pseudo first order kinetics and provided a U-shaped pH-rate profile with an apparent pH-independent region between pH values of approximately 4 to 7. The products of degradation varied such that the overall loss of PIV-PR-020 was a complex function of both parallel and consecutive reactions with clear indications of reversible isomerization occurring starting around pH 7. The degradation of PIV-PR-020 in aqueous solution was found to be both acid catalyzed below pH 4 and base catalyzed above pH 7. The data shows that the acid catalyzed α-keto-epoxide ring opening appears to be an SN_2 reaction (concerted reaction) since the reaction rate and products were sensitive to changes in halide concentrations. While under basic pH conditions, insufficient data was available to establish if the α-keto-epoxide ring opening was due to and SN_2 or SN_1 reaction.

It has also been shown that there is some scrambling at the carbon at the C_1 position at higher pH values due to base catalyzed isomerization. At these higher pH values, there are two diols formed, the (S,R) diol, and the (R,R) diol. The disappearance plots of PIV-PR-020 at pH 8 do not follow pure first order

behavior as deviations were seen at later times. This is expected, as the isomerization reaction is a reversible process. No effort was made to curve fit the data due to the complexity of the reaction pathways (16). In addition during the course of this study, the concentration of the PIV-PR-020 and its diastereomer at the higher pH values begins to decrease. Concurrently, both of the two diols are formed with (R,R) diol showing a lag-phase. This is consistent with its formation from the diastereomer.

During the course of the study, the temperature, ionic strength, buffer concentration, and halide effect were evaluated while keeping the concentration of the reactant constant. No major buffer strength effect was observed, which suggested no general acid and general based catalyzed reaction.

Loss of PIV-PR-020 was significantly affected by the halide counter-ion in the salt used to maintain the constant ionic strength. As the nucleophilicity of the halide increased, as per the Swain-Scott n value, so did the reaction rate.

Not all of the degradation products for the loss of PIV-PR-020 were identified. At low pH values, there are early eluting degradation products with a molecular weight, based on LCMS analysis, consistent with the molecular weight of the diols. This molecular weight, being the same as the diols, may have been due to dehydration reactions in the MS. The specific structures of these early eluting products were not identified during the course of this study. At higher pH values, the rate equations are also complex not only due to parallel reactions, but also the reversible nature of the isomerization reaction. Mass balance was conserved over the first approximate 25% of PIV-PR-020 loss but there was a loss

in mass over the course of the reaction at the higher pH values and at longer time points suggesting significant secondary degradation was occurring.

References

1. *Method Development for the seperation of a Proteasome Inhibitor, Oprozomib, and Related Substances.* **Garg, A., et al., et al.** 2013. American Association of Pharmaceutical Sciences.
2. *Design and Sythesis of an Orally Bioavailable and Selective Peptide Epoxyketone Proteasome Inhibitor (PR-047).* **Zhou H, Aujay MA, Bennett MK, Dajee M, Demo SD, Fang Y, Ho MN, Jiang J, Kirk CJ, Laidig GJ, Lewis ER, Lu Y, Muchamuel T, Parlati F, Ring E, Shenk KD, Sheilds J, Shwonek PJ, Stanton T, Sun SM, Sylvain C, Woo TM, Yang J.** 2009, Journal of Medicinal Chemistry, pp. 3028-3038.
3. *New Proteasome Inhibitors in Myeloma.* **Panisinee Lawsut, Dharminder Chauhan, Jacob Laubach, Catriona Hayes, Claire Fabre, Michelle Maglio, Constantine Mitsiades, Teru Hideshima, Kenneth C. Anderson, Paul G. Richardson.** 2012, Current Hematol Malig Rep, Vol. 7, pp. 258-266.
4. *Crystal Structure of Epoxomicin:20S Proteasome Reveals a Moleculare Basis for Selectivity of ά, β-Epoxyketone Proteasome Inhibitors.* **Grol M, Kim KB, Kairies N, Huber R, Crews CM.** 2000, Journal of the AMerican Chemical Society, pp. 1237-1238.
5. *Epoxide Hydrolase-Catalyzed Enantioselective Synthesis of Chiral 1,2-Diols via Desymmetrization of meso-Epoxides.* **Zhao L, Han B, Miller M, Huang H, Malashock D, Zhu Z, Milan A, Robertson D, Weiner DP, Burk M.** 2004, Journal of the American Chemical Society, Vol. 126, pp. 11156-11157.
6. *Functional Group Selectivity in Reactions of Epoxides with Tungsten Hexachloride.* **Michael E. Jung, Jennifer M. Murphy.** 207, Tetrahedron Letters, Vol. 48, pp. 8388-8391.
7. *Mechanistic Investigation Leads to a Synthetic Improvement in the Hydrolytic Kinetic Resolution of Terminal Epoxides.* **Nielsen, Lars P.C., et al., et al.** 2004, Journal of the American Chemical Society Communications, Vol. 126, pp. 1360-1362.
8. *Compared Behaviors of trans- and cis-α,β-Epoxy-γ,δ-vinyl-salines Towards Nucleophiles and Bases: High Regioselective Ring Opening and Deprotonation.* **Marié JC, Courillon C, Malacria M.** 2002, Synlett, Vol. 4, pp. 553-556.
9. *A novel boron trifluoride etherate mediated deep-seated rearrangement of an a-b epoxyketone.* **Srikrishna A, Ramasastry S.** 2005, Tetrahedron: Asymmetry, Vol. 16, pp. 2973-2989.
10. **Eric V. Anslyn, Dennis A. Dougherty.** *Modern Physical Organic Chemistry.* Sausalito, Clifornia : University Science Books, 2006.
11. **Ege, Seyhan N.** *Organic Chemistry, Second Edition.* Lexington, Massachusetts : D.C. Heath and Company, 1989.
12. *Quantitative Correlation of Relative Rates. Comparison of Hydroxide Ion with Other Nucleophilic Reagents towards Alkyl Halides, Esters, Epoxides and Acyl Halides.* **Swain, C. Gardener and Scott, Carlton B.** Jan 5, 1953, Vol. 75, pp. 141-147.
13. *Nucleophilic Reactivities towards Cations.* **Ritchie, Calvin D.** 1972, Journal of American Chemical Society, Vol. 94, p. 3275.

14. *Pressure Effect and Mechanism in Acid Catalsis Part 3 - Hydrolysis of epoxides.* **Whalley, J. Koskokallio and E.** 1959, Transactions of the Faraday Society, Vol. 55, pp. 815-823.
15. *Synthetic Catalysis of Amide Isomerization.* **Christopher Cox, Thomas Lectka.** 12, 2000, Accounts of Chemical Research, Vol. 33, pp. 849-858.
16. **Connors, Kenneth A.** *Chemical Kinetics.* New York : VCH Publishers, Inc., 1990. 1-56081-053-X.
17. *Definition of a Nucleophilicity Scale.* **Paula Jaramillo, Patricia Perez, Renato Contreras, William Tiznado, Patricio Fuentealba.** Jul 6, 2006, The Journal of Physical Chemistry , Vol. 26, pp. 8181-8187.
18. *Base Catalyzed Isomerization of Phenylpropenes.* **M. Hassan, A. R. O. Abdel Nour, A. M. Satti, K. S. Kirollos.** 1982, International Journal of Chemical Kinetics, Vol. 14, pp. 351-356.

Appendix

Supplimental data

Synthesis Procedure

PIV-PR-020 (S,R)

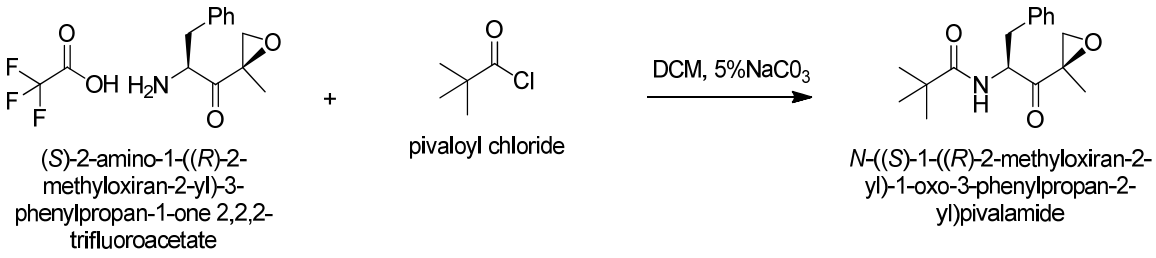

(*S*)-2-amino-1-((*R*)-2-methyloxiran-2-yl)-3-phenylpropan-1-one 2,2,2-trifluoroacetate

N-((*S*)-1-((*R*)-2-methyloxiran-2-yl)-1-oxo-3-phenylpropan-2-yl)pivalamide

Into a 250 mL round bottomed flask was added (S)-2-amino-1-((R)-2-methyloxiran-2-yl)-3-phenylpropan-1-one 2,2,2-trifluoroacetate (10.0 g, 31.3 mmol) and dichloromethane (100 ml). The solution was cooled to < 5 °C and saturated sodium bicarbonate (50 ml) was added, followed by slow addition of pivaloyl chloride (4.91 g, 407 mmol) at a rate maintaining less than 10 °C. After the biphasic solution was stirred for 10 min the reaction was determined to be complete by TLC. The organic phase was washed with water , brine, dried with magnesium sulfate, filtered and concentrated to an oil. The oil purified by silica gel flash column chromatography eluting with ethyl acetate and heptanes. The material was then recrystallized hot from *tert*-butymethy ether and heptanes providing 6.26 g (69% yield) of *N*-((*S*)-1-((*R*)-2-methyloxiran-2-yl)-1-oxo-3-phenylpropan-2-yl)pivalamideas a white powder. HPLC indicated that the purity was 99.8% pure.

PIV-PR-020 (S,R) chlorohydrin

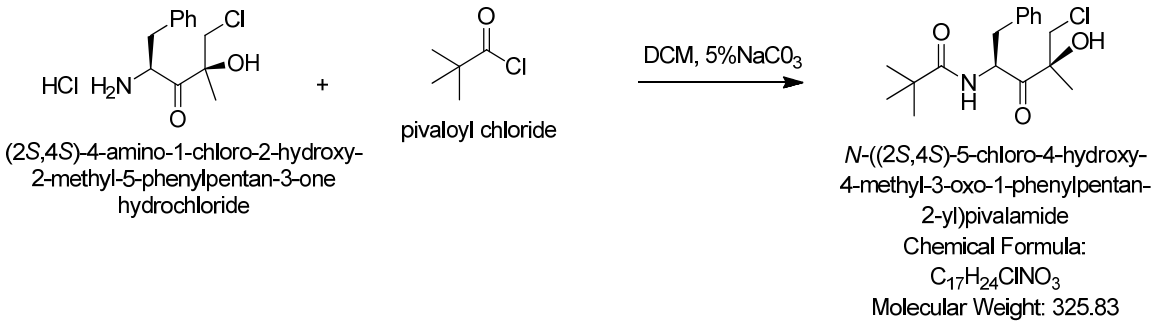

(2*S*,4*S*)-4-amino-1-chloro-2-hydroxy-2-methyl-5-phenylpentan-3-one hydrochloride

N-((2*S*,4*S*)-5-chloro-4-hydroxy-4-methyl-3-oxo-1-phenylpentan-2-yl)pivalamide
Chemical Formula: $C_{17}H_{24}ClNO_3$
Molecular Weight: 325.83

Into a 50 mL round bottomed flask was added (2*S*,4*S*)-4-amino-1-chloro-2-hydroxy-2-methyl-5-phenylpentan-3-one hydrochloride (1.00 g, 0.35 mmol), dichloromethane (10 ml), and pivaloyl chloride (0.58 g, 4.7 mmol). To the suspension was added saturated sodium bicarbonate (20 ml) and the solution was allowed to stir at for 8h at 20 °C. The phases were separated and the organic phase was washed with 10% $NaHSO_4$, 5% $NaHCO_3$, brine, dried with sodium sulfate, filtered and concentrated to an oil. The oil was purified by silica gel flash column chromatography eluting with ethyl acetate and heptanes. The resulting material was then recrystallized from hot ethyl acetate and heptanes, providing *N*-((2*S*,4*S*)-5-chloro-4-hydroxy-4-methyl-3-oxo-1-phenylpentan-2-yl)pivalamide as a white powder in 68% yield (0.68g). HPLC indicated that the purity was > 99.5% pure.

PIV-PR-020 (S,R) diol

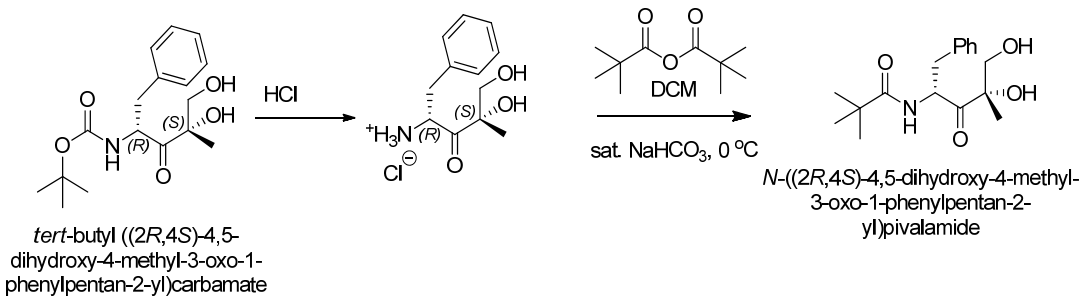

A solution *tert*-butyl ((*2R*,*4S*)-4,5-dihydroxy-4-methyl-3-oxo-1-phenylpentan-2-yl)carbamate (2.0 g, 6.18 mmol) in dichloromethane (3.0 ml) was treated with 4 N HCl in dioxane (5.0 mL, 20.0 mmol). The resulting mixture was concentrated. The residue was suspended in DCM (20 mL) and cooled to 0 °C and then pivaloyl chloride (1.43 g, 11.86 mmol) and saturated sodium bicarbonate (20 ml) were added. The organic phases were separated and the organic phase was concentrated to a crude solid. The solid was recrystallized from heptanes, providing *N-((2R,4S)*-4,5-dihydroxy-4-methyl-3-oxo-1-phenylpentan-2-yl)pivalamide as a white powder. HPLC indicated that the purity was 96.0% pure.

PIV-PR-020 (R,R) diastereomer

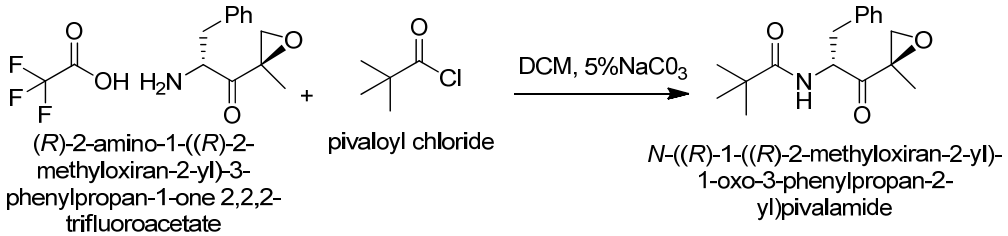

A solution of (*R*)-2-amino-1-((*R*)-2-methyloxiran-2-yl)-3-phenylpropan-1-one 2,2,2-trifluoroacetate (100 mg, 0.313 mmol) and pivaloyl chloride in

dichloromethane was cooled to in an ice bathe then treated with saturated sodium bicarbonate. The organic phase was concentrated and the residue recrystallized form heptanes providing *N*-((*R*)-1-((*R*)-2-methyloxiran-2-yl)-1-oxo-3-phenylpropan-2-yl)pivalamide as a white powder. HPLC indicated that the purity was 98.6%pure.

PIV-PR-020 (R,R) diol

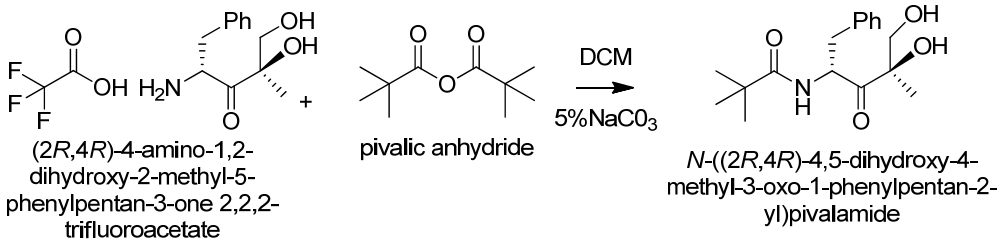

(2*R*,4*R*)-4-amino-1,2-dihydroxy-2-methyl-5-phenylpentan-3-one 2,2,2-trifluoroacetate

N-((2*R*,4*R*)-4,5-dihydroxy-4-methyl-3-oxo-1-phenylpentan-2-yl)pivalamide

A solution of (*2R,4R*)-4-amino-1,2-dihydroxy-2-methyl-5-phenylpentan-3-one 2,2,2-trifluoroacetate (1.00 g, 2.95 mmol), saturated sodium bicarbonate (10ml), and dichloromethane (10.0 ml) were cooled to 0 °C, then pivaloyl anhydride (1.27 mmol) was added slowly. The organic phase was extracted with 5% citric acid and brine, then dried with sodium sulfate, filtered, and concentrated. The residue was then purified by flash column chromatography providing *N*-((*2R,4R*)-4,5-dihydroxy-4-methyl-3-oxo-1-phenylpentan-2-yl)pivalamideas a white powder. HPLC indicated that the purity was 82.6%pure.

LCMS of Synthesized Materials

PIV-PR-020, PIV-PR-020 (R,R) diastereomer, PIV-PR-020 (S,R) diol, PIV-PR-020 (R,R) diol, and PIV-PR-020 (S,R) chlorohydrin were run by HPLC and LCMS. The HPLC chromatograms showed no addition peaks (data not shown). The LCMS clearly show the correct molecular weights for the m+1 and m+23 (sodium). There are additional higher molecular weight peaks on the PIV-PR-020 (R,R) diastereomer, PIV-PR-020 (R,R) diol, and PIV-PR-020 (S,R) chlorohydrin which correspond to the addition of the m+1 mass and the m+23 mass. This may be due to dimerization in the LCMS. PIV-PR-020 shows a smaller peak with a molecular weight which corresponds to the pivoyl-amide fragment of the structure.

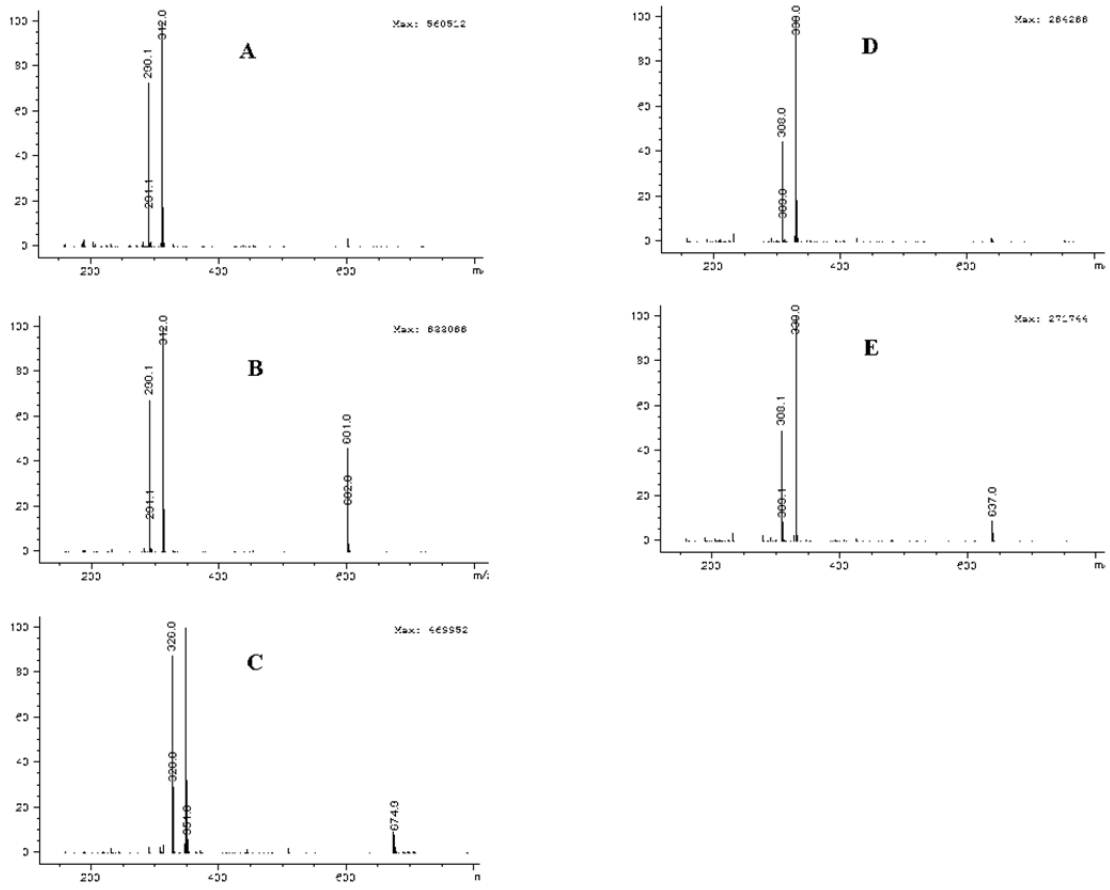

Figure A. LCMS of (A) PIV-PR-020 with the S,R S(C_1), R (C_3) stereochemistry and its proposed degradation products (as standards), (B) PIV-PR-020 (R,R) diastereomer, (C) PIV-PR-020 (S,R) chlorohydrin, (D) PIV-PR-020 (S,R) diol, and (E) PIV-PR-020 (R,R) diol.

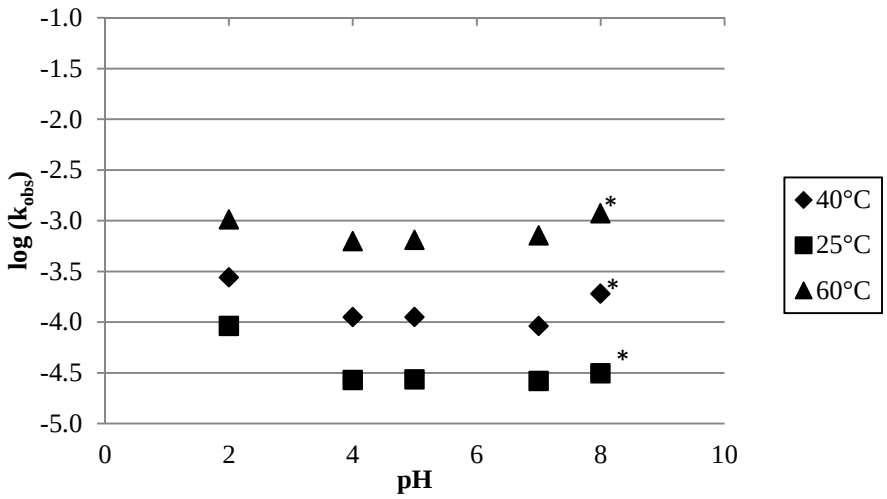

Figure B. pH-Rate profile for the degradation of PIV-PR-020 at 25°C, 40°C, and 60°C in aqueous buffers with the ionic strength adjusted to 0.15 with sodium chloride. * pH 8 value is an approximation since it does not follow pure first order kinetics throughout the full time course of the study.

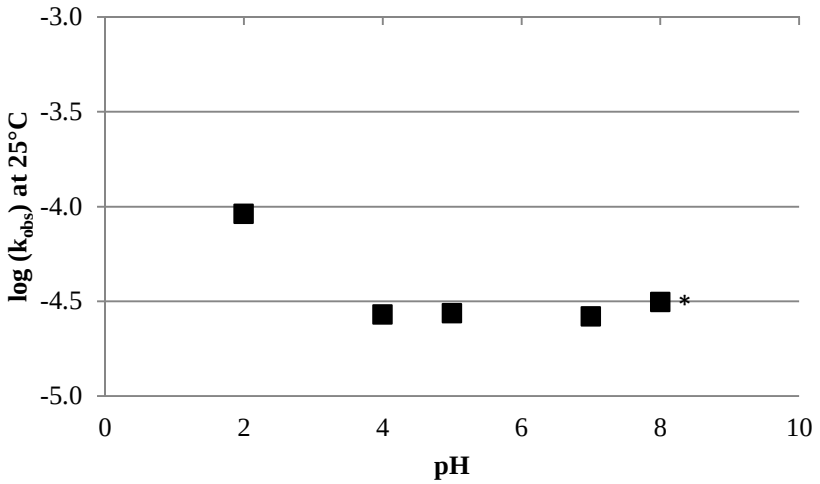

Figure C. pH-Rate profile for the degradation of PIV-PR-020) at 25°C in aqueous buffers with the ionic strength adjusted to 0.15 with sodium chloride. * pH 8 value is an approximation since it does not follow pure first order kinetics throughout the full time course of the study.

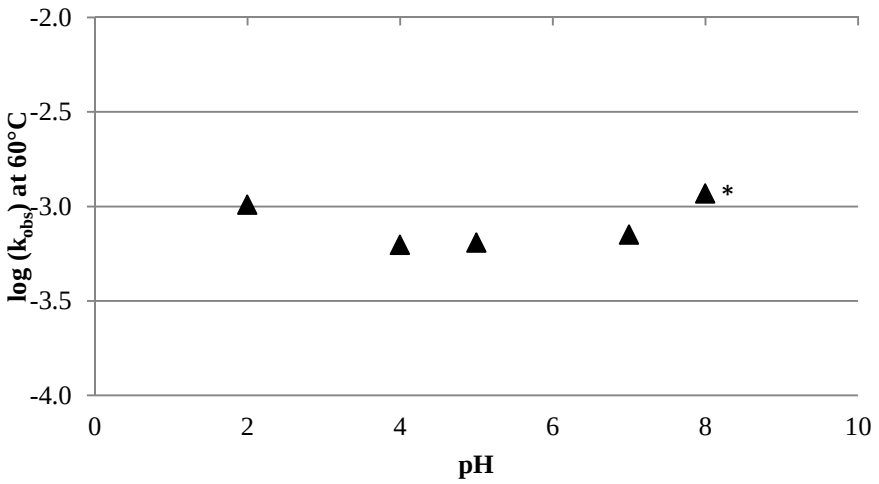

Figure D. pH-Rate profile for the degradation of PIV-PR-020 at 60°C in aqueous buffers with the ionic strength adjusted to 0.15 with sodium chloride. * pH 8 value is an approximation since it does not follow pure first order kinetics throughout the full time course of the study.

pH_{app}	k_{obs} (min^{-1})		
	25°C	40°C	60°C
2	9.15×10^{-05}	2.74×10^{-04}	1.02×10^{-03}
4	2.69×10^{-05}	1.11×10^{-04}	6.24×10^{-04}
5	2.73×10^{-05}	1.11×10^{-04}	6.43×10^{-04}
7	2.63×10^{-05}	9.10×10^{-05}	7.07×10^{-04}
8*	3.13×10^{-05}	1.89×10^{-04}	1.17×10^{-03}

Table A. Observed first-order rate constant values, k_{obs}, for loss of PIV-PR-020 at pH values of 2, 4, 5, 7, and 8 by HPLC at 25°C, 40°C, and 60°C. Observed rate constants were calculated as the slopes of the natural logarithm of the concentration of PIV-PR-020 versus time. * pH 8 value is an approximation since it does not follow pure first order kinetics throughout the full time course of the study.